Analytica Chimica Acta 1085 (2019) 91–97

Contents lists available at ScienceDirect

Analytica Chimica Acta

journal homepage: www.elsevier.com/locate/aca

Nanoporous gold electrode for ultrasensitive detection of neurotoxin fasciculin

Xiao Hu, Cerasela Zoica Dinu*

Department of Chemical and Biomedical Engineering, West Virginia University, Morgantown, 26506, WV, United States

HIGHLIGHTS

- Nanoporous gold electrode with increased electrochemically active area was fabricated.
- Acetylcholinesterase was efficiently immobilized at the electrode interface.
- The electrode showed high detection capability (8 pM) of fasciculin neurotoxin after only 30 min incubation.
- Created biosensor was accurate and very selective for the detection of fasiculin.

GRAPHICAL ABSTRACT

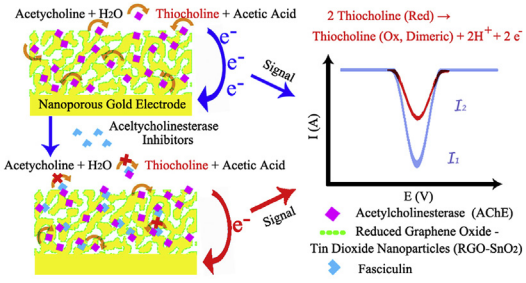

ARTICLE INFO

Article history:
Received 10 May 2019
Received in revised form
11 July 2019
Accepted 30 July 2019
Available online 2 August 2019

Keywords:
Acetylcholinesterase
Biosensor
Neurotoxin
Fasciculin
Ultra detection

ABSTRACT

Acetylcholinesterase (AChE), an efficient biocatalyst known to hydrolyze the neurotransmitter acetylcholine, could be inactivated in the presence of insecticides, nerve agents or other drug inhibitors to thus result in disrupted neurotransmission. Improvement in the peripheral cholinergic function, as well as overall cognition and neuronal functions of an exposed system could be achieved if the mechanisms of inhibitions are deactivated in a controlled fashion and with rapid response time. Herein, we proposed to develop a simple AChE biosensor capable to realize the rapid detection of neurotoxins. Our approach uses a nanoporous gold film (NPGF) and reduced graphene oxide-tin dioxide nanoparticle (RGO-SnO_2) nanocomposite to define the highly active electrode interface where the electrochemical monitoring of the interaction between AChE and its target molecule, fasciculin, could take place. Our results demonstrate that the established biosensor had the ability to monitor fasciculin concentrations at the ultra-low limit of detection of 8 pM, an inhibition rate of 8% and within only 30min of electrochemical exposure. Our study provides a convenient technology for the rapid and ultrasensitive detection of neurotoxins and has the potential for large applicability to other drugs or toxins screening.

1. Introduction

Alzheimer's disease is one of the most common causes of dementia in an aging population, with 1 in about 10 people over age 65 being affected and with approximately 200,000 Americans under the same age showing onset disease symptoms [1]. Even though the disease is known to progressively impair cognitive

* Corresponding author. Department of Chemical and Biomedical Engineering, West Virginia University, Benjamin M. Statler College of Engineering and Mineral Resources, PO Box 6102, Morgantown, WV, 26506, USA.
E-mail addresses: cerasela-zoica.dinu@mail.wvu.edu, czdinu01@gmail.com (C.Z. Dinu).

https://doi.org/10.1016/j.aca.2019.07.067
0003-2670/

functions, its early diagnosis and effective treatment have been challenging.

Previous research has showed that acetylcholinesterase (AChE) inhibitor drugs could potentially offer a viable treatment option; AChE is known to regulate cholinergic pathways [2] and contributes to reliable cognitive functions such as the ones identified in impaired Alzheimer patients. Improvement in Alzheimer's disease symptoms was, for instance, observed after donepezil hydrochloride (one AChE inhibitor) was administered in clinical tests, with the amounts of systemic cholinergic effects being dose-depend on the inhibitor [3] as well as its specific AChE's binding mechanisms. Substantial evidence also showed that drugs such as galantamine and rivastigmine could decrease the activity of AChE [4]. Complementary, natural AChE inhibitors found in plants, fungi and snake venoms were shown to have a high affinity and ensure a reversible inhibition of AChE. For instance, fasciculin, a natural inhibitor isolated from snake venom was revealed to have an inhibitory constant (K_i) in the range of 10^{-11}–10^{-12} M [5]. Fasculin binding to AChE is known to occur through its cluster of hydrophobic residues located in the loop II of the molecule, with such loop's association to the peripheral anionic site of the AChE leading to sterical occlusion of the substrate's (i.e., acethylcoline-ACh) access to the molecule's catalytic site. The binding is highly efficient, with studies revealing that small amounts of intraperitoneal injections (i.e., 0.5−3 μg/g body weight) administered to mice could decrease AChE activity up to 45−60% [6]. However, even though such treatment options have considerable potential, there are still concerns about possible safety issues at drug's administration, with studies recording induced malfunction of AChE associated with respiratory problems, myocardial malfunctioning, and even death [7]. In particular, it was shown that since fasciculin is isolated from snake venom it could cause acute health effects at even pM concentrations of administration [8], with specific studies revealing that injection of fasciculin to mice led to hypersensitivity to touch and sever and long lasting (up to 4~7 h) fasciculations such as salivation, lacrimation and uncontrolled muscle twitches. Considering that AChE levels could vary between 26.7 and 21.1 mU/mL in individuals with Alzheimer and further, considering that for a specific patient the AChE levels could be altered during the different stages of the disease and treatment [9] with its levels being known to increase around β-amyloid plaques, it is imperious to strictly control both the dosage of fasciculin as well as AChE metabolic levels [10]. This suggests that identifying both the therapeutic and the toxicity windows and how they depend on the AChE binding affinity, as well as ensuring rapid drug transfer into the blood as well as rapid detection of any deleterious effects that such drug could produce needs to be considered if future implementation of fasciculin or other similar compounds is to be undertaken.

We proposed the design and fabrication of a user-friendly platform that could allow monitoring of both fasciculin binding to AChE as well as its dosage. Our method relied on a simple, rapid and effective biosensorial platform. Biosensing platforms are rapid and convenient methods for trace amount detection of biological molecules [11] or drugs [12,13]. Our biosensor allowed for rapid response upon monitoring the affinity of the inhibitor binding down to pM concentrations, low detection limit, convenience and cheapness. Our results showed that the developed method does not only eliminate the slow response or laborious setup required by current strategies relying on fluorescent biosensor or colorimetric determination, but further, it has a high level of specificity thus eliminating the rather poor or non-specific binding encountered with the above listed strategies [14]. The potential of our proposed method is foreseen for clinical implementation, with the established platform to be used for pre-screening of other drugs to thus help identify toxicity or treatment doses options in a short time and under real-time conditions, all while limiting the costs and possible drug' side effects.

2. Materials and methods

2.1. Nanoporous gold film (NPGF) electrode fabrication and evaluation

A gold (Au) electrode (CH Instruments Inc) was cleaned by immersion in Piranha solution (96.4% sulfuric acid, H_2SO_4, and 30% hydrogen peroxide, H_2O_2, Fisher Scientific, in a 3:1 (v:v)) at 120 °C for 10 min. The electrode was subsequently rinsed with deionized (DI) water and polished successively with 1.0, 0.3 and 0.05 μm α-alumina powders (CH Instrument Inc.) until a mirror-like surface was obtained. Impurities were removed by rinsing with DI water. The electrode was subsequently sonicated in 10 mL ethanol (99.5%, Fisher Scientific), acetone (99.5%, Fisher Scientific) and DI water sequentially, for 5 min each cycle. The cleaned electrode was further activated in H_2SO_4 by applying multiple electrochemical oxidation-reduction cycles, with the applied potential being cycled from 0.4 to 1.6 V (vs. silver/silver chloride electrode - Ag/AgCl, CH Instrument Inc.) at a scan rate of 100 mV/s on a VersaSTAT 3 potentiostat/galvonostat (Princeton Applied Research) using a platinum (Pt, CH Instrument Inc.) electrode as the auxiliary unit. The process was repeated until the cyclic voltammetry graph became stable.

Upon the treatment, the electrode was rinsed thoroughly with DI water and blown dry, then used for preparing a NPGF onto its surface. For this, a multi-cyclic alloying/dealloying process was carried out from 1.45 to −0.70 V in an electrolyte of benzyl alcohol (BA, 98%, Fisher Scientific) containing 1.6 M zinc chloride ($ZnCl_2$, Fisher Scientific) for 30 cycles, at 120 °C and under a scan rate of 10 mV/s. Herein the electrolyte used to make the nanoporous structure was prepared by dissolving 2.18 g $ZnCl_2$ in the 10 mL BA at 60 °C. Zn wires (d = 0.5 mm, 99.994%, Alfa Aesar) were used as counter electrode and reference electrode. The cleaned activated electrode formed the working electrode. Thus prepared NPGF electrode was sonicated sequentially in 10 mL BA, ethanol and DI water for 5 min each cycle, then activated again in the 50 mM H_2SO_4 (as described above), rinsed with DI water and blown dry before use.

2.2. NPGF surface characterization

The morphology of the user-prepared NPGF electrode was characterized using an Atomic Force Microscope (AFM, Nikon, USA) in contact mode. The cantilever spring constant was calibrated using the thermal noise method; the scan rate was fixed at 0.5 Hz for all the experiments.

2.3. Synthesis of reduced graphene oxide (RGO)

RGO nanosheets were synthesized according to established protocol [15]. Briefly, graphene oxide (GO) was first prepared by the Hummers' method in which 0.5 g graphite (Fisher Scientific) and 0.38 g sodium nitrite ($NaNO_3$, Fisher Scientific) were mixed and dissolved in 38 mL H_2SO_4 all in an ice-water bath. Subsequently, 0.23 g potassium permanganate ($KMnO_4$, Fisher Scientific) was slowly added into the mixture, with gentle stirring (about 50 rpm) on a hotplate (VWR International Inc.) over a 1 h time period. The mixture was again stirred gently for another 2 h in an ice-water bath, then stirred vigorously for 5 additional days on a stirring plate, at 1000 rpm and room temperature. Upon stirring, 70 mL of 5% H_2SO_4 was added into the mixture. The resulting products were centrifuged at 3000 rpm for 30 min, washed thoroughly with DI

water and dried in vacuum, overnight. The GO sheets were dissolved again in the DI water (0.1 mg/mL) with the pH being adjusted to 11 using a 5% ammonia aqueous solution ($NH_3 \cdot H_2O$, Fisher Scientific). As the reducer, hydrazine hydrate (55%, Fisher Scientific) was added into the mixture (1 μL hydrazine hydrate to 3 mg GO) and incubated at 80 °C for 12 h, again with stirring. The resulting RGO nanosheets were again centrifuged at 3000 rpm for 30 min, washed thoroughly with DI water and dried in vacuum overnight.

2.4. Fabrication of the acetylcholinesterase biosensor (AChE)

The cleaned NPGF electrode was used to fabricate an AChE biosensor. For this, nanocomposites were first prepared by dispersing a mixture of 6 mg tin dioxide (SnO_2, Sigma) nanoparticles and 1 mg RGO nanosheets (mass ratio of 6:1) in 1 mL 1% acetic acid (99.7%, Fisher Scientific) with 0.2% chitosan (Fisher Scientific). The nanocomposites were stirred at room temperature for 3 h. Secondly, 10 μL of such solution were dropped onto the working electrode and kept overnight at room temperature. Thirdly, 10 μL of 50 μg/mL AChE (Sigma) was dropped onto the nanocomposite functionalized electrode and incubated overnight at 4 °C. The electrode was subsequently rinsed with 50 mM phosphate buffered saline (PBS, Fisher Scientific, pH 7.0) and blown dry. Ten μL of fasciculin (Abcam, concentrations varied from 0.1 pM to 10 nM) were dropped onto the functionalized electrode and incubated for 30 min at room temperature. Then, another 10 μL of 0.25% Nafion (Fisher Scientific) were dropped onto the electrode and incubated for another 30 min at room temperature. The prepared modified electrode was rinsed thoroughly with PBS to remove any impurities.

2.5. Electrochemical measurement

All electrochemical measurements were carried out in ambient atmosphere. A Pt wire was used as the auxiliary electrode, Ag/AgCl as the reference and the NPGF electrode or modified NPGF electrodes (RGO-SnO_2/NPGF, AChE/RGO-SnO_2/NPGF and fasciculin/AChE/RGO-SnO_2/NPGF electrode respectively) were used as working electrodes. Differential pulse voltammetry (DPV) and electrochemical impedance spectrum (EIS) were recorded on the VersaSTAT 3 potentiostat/galvonostat. For the DPV, the voltage ranged from 0.4 to 0.8 V with a 50 ms pulse, 49 ms pulse width, 50 mV pulse height and 1 mV pulse potential increment. DPV analyses were performed in different concentrations of acetylcholine chloride (Fisher Scientific, 16 μM to 50 nM) in 50 mM PBS containing 10 mM potassium chloride (KCl, Fisher Scientific). For the EIS, the frequency ranged from 0.01 to 100000 Hz; 5 mV amplitude was maintained constant. The EIS analyses were performed in 50 mM potassium ferrocyanide ($K_3Fe(CN)_6$, Fisher Scientific) dispersed in 50 mM PBS containing 10 mM KCl.

3. Results and discussion

3.1. Preparation and characterization of the nanoporous gold film (NPGF) electrode

We designed a strategy to evaluate the binding mechanisms of fasciculin to acetylcholinesterase (AChE); fasciculin is an AChE natural inhibitor that could potentially offer a viable treatment for regulation of cholinergic pathways in impaired Alzheimer patients. By allowing real-time, sensorial detection, our strategy aims to discriminate how structural conformation changes of AChE resulted from fasciculin binding could lead to poor clinical outcome [14].

We first hypothesized that a NPGF electrode could be used to increase the detection of such binding mechanisms, since previous research showed that NPGF electrodes have a higher surface area and thus allow for a better electron transport profile at their interfaces to thus provide a great number of adsorption sites when biomolecules analyses are considered [16].

The NPGF electrode was prepared using a multicycle alloying/dealloying process shown in Fig. 1 (a). The zinc cation (Zn^{2+}) in the electrolyte was firstly reduced to Zn on the electrode's surface and formed the Au-Zn alloy at the electrode's interface. Subsequently, during the dealloying process, the deposited Zn was dissolved into the electrolyte to favor higher reactivity [17]. Such process could potentially lead to pores formation at the electrode surface, with the severity of the pores to be associated with the number of alloying/dealloying cycles. Fig. 1 (b) shows the side view of the Au (control) and prepared NPGF electrode, while Fig. 1 (c) shows the CV of the alloying/dealloying processes at the electrode interface. As revealed, the potential ranged from −0.72 to −1.45 V, with two anodic peaks appearing at about 0.56 and 0.93 V respectively; a noticeable reduction wave was observed at about 0.52 V presumably due to the Zn deposition [18]. The first anodic peak appeared at about 0.56 V and represents the oxidation of the deposited Zn [18], while the second peak at about 0.93 V was attributed to the oxidation of Zn in the Au-Zn alloy [18]. Changes in surface morphologies were confirmed by AFM, with analysis (Fig. 1 (d) and (e)) showing that the NPGF electrode had a rougher surface relative to that of control Au, with the roughness factor (Rf; known to equals the ratio of the real electrochemically reactive surface area and the geometrical area) being 25.39 for the Au electrode and 91.26 for the NPGF one respectively. In addition, Fig. 1 (f) showed that the surface of the NPGF was about 100 nm higher than that of the control.

The NPGF electrode was further characterized using a potentiostat/galvanostat; Fig. 2 (a) and (b) show the electrochemical behaviors of NPGF and Au control electrodes respectively. Specifically, two oxidation peaks (at about 1.1 and 1.3 V) and one reduction peak (at about 0.90 V) appeared on the CV curves of the NPGF electrode; the peaks corresponded to the Au oxidation and Au oxide reduction respectively. Analysis showed that the reduction peak increased greatly relative to that of the Au electrode thus confirming the AFM results and induced changes in the electrochemically reactive surface area [19,20]. Indeed, the electrochemically reactive surface areas of the Au and NPGF electrodes calculated by using the charge in the Au oxide reduction peak (Fig. 2 (a)) divided by the charge passed per unit surface area (390 μC/cm^2 for Au) [21], were about 0.8 and 2.9 cm^2 respectively. Moreover, the electrochemical behaviors of the $Fe(CN)_6^{3-/4-}$ at the Au and NPGF electrodes (Fig. 2 (b)) also revealed the much greater oxidation and reduction peaks for the modified electrode, with the peak current at the NPGF electrode being about 16 times that of the Au one.

3.2. AChE biosensor fabrication and performance testing

The NPGF electrode was used as a substrate for active deposition of reduced graphene oxide (RGO) containing tin dioxide (SnO_2) dopants (Fig. 3 (a)). Our hypothesis was that the known conductivity, high surface area and known facilitated ionic/mass transport of RGO [22] will enhance the selection sensitivity at the NPGF electrode's interface. Further, we also hypothesized that addition of SnO_2 could increase electrode's sensitivity [23]. Previous research in RGO amperometric glucose biosensors showed a sensitivity of 12.5 mA mM^{-1} cm^{-2} conferring to such fabricated electrode a short response time of less than 1 s and an ultralow detection limit of 5 nM respectively [24]. Moreover, the RGO-based acetylcholinesterase biosensor used for amperometric detection of organophosphorus pesticides showed a limit of detection of 1.3 pM [25]. Complementarily, SnO_2-based biosensors showed good performances for glucose detection [26] at concentrations as low as 4.5

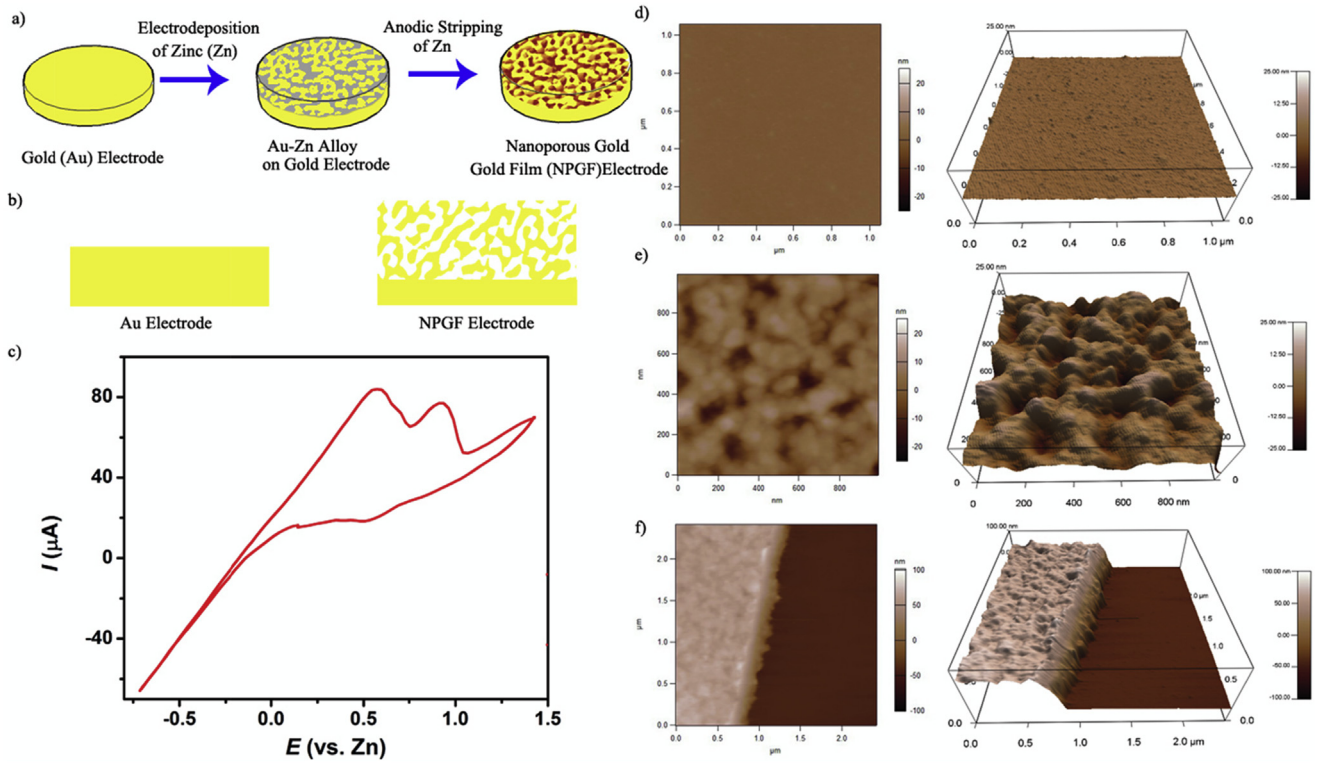

Figure 1. (a) Scheme of the NPGF electrode prepared using an electrochemical alloying/dealloying strategy. Briefly, a cleaned Au electrode was immersed in an electrolyte of benzyl alcohol with zinc chloride. Zn was firstly electrodeposited onto the Au electrode to form an Au-Zn alloy and subsequently dealloyed to form a porous electrode surface. (b) Schematics of the side views of the Au and NPGF electrodes respectively. (c) The 10-th cyclic voltammetry (CV) of the alloying/dealloying process. (d) Representative Atomic Force Microscopy (AFM) morphology analyses of the Au electrode (control). NPGF electrode (e), and interface of Au and NPGF respectively (f).

pM. In our experiment, it was expected that SnO_2 binds to RGO through electrostatic interactions to increase charge transfer at its interface [27], with RGO to also increase the overall surface area and porosity of the electrode based on its sheet-like geometry (Supporting Information Fig. S1), thus allowing for increased binding at the electrode interface.

The modified electrode was used to detect binding mechanisms of fasciculin to AChE through known redox reactions. Specifically, it was hypothesized that if the immobilized AChE would catalyze the acetylcholine (Ac) to thiocholine reaction [28], the thiocholine would then show an oxidation reaction and generate an electrochemical signal at electrode's interface as shown in Equations (1) and (2) below:

$$Acetylcholine + H_2O \overset{AChE}{\rightarrow} Thiocholine + Acetic \quad Acid \tag{1}$$

$$2Thiocholine \quad (red) \rightarrow Thiocholine \quad (ox,\ dimeric) + 2H^+ + 2e^- \tag{2}$$

It was also assumed that produced thiocholine would generate an electrochemical signal that could correlate with the amount of the AChE and the concentration of the Ac in the electrolyte respectively. Lastly, any subsequent addition of fasciculin was expected to lead to fasciculin's binding to the AChE, blocked enzymatic reaction and reduced signal at the electrode interface.

Indeed, analysis showed that when fasciculin was added to the experimental setup, a decrease in the generated electrochemical signal (Fig. 2 (c)) was recorded. Analysis of Nyquist plots at the NPGF, RGO-SnO_2/NPGF, AChE/RGO-SnO_2/NPGF and Fasciculin/AChE/RGO-SnO_2/NPGF electrodes respectively (Fig. 2 (d)) showed that the semicircle portion at higher frequencies of such plots is caused by the electron transfer limited process, while the linear portion recorded at lower frequencies corresponds to a diffusion process [29]. The electrochemical impedance spectrum (EIS) revealed that the resulting Nyquist plots were almost straight lines for both the NPGF and RGO-SnO_2/NPGF electrodes, suggesting that the redox reactions at these electrodes' interfaces were mainly controlled by diffusion processes. The slope of the linear portion on the RGO-SnO_2/NPGF electrode however decreased when compared with the slope on the NPGF electrode, presumably due to the effect being strengthened after the immobilization of the RGO-SnO_2 nanocomposite and the increase in the available electrode surface area that they will produce. Further, Nyquist plots at the AChE/RGO-SnO_2/NPGF and Fasciculin/AChE/RGO-SnO_2/NPGF electrodes revealed both semicircle and linear portions with the diameter of the semicircles representing the values of the electron transfer resistances (R_{ct}) being about 45 and 60 kΩ respectively. Binding of fasciculin to the AChE, as expected, hindered the electron transfer thus increasing the R_{ct} (about a 33.3% increase). Oxidation peaks appeared at about 0.58 V after the AChE was immobilized onto the electrode and were attributed to the oxidation of the triocholine as described in the reactions (1) and (2) above.

3.3. Fasciculin sensing and biosensor validation

Upon electrode's incubation in a solution of fasciculin for 30 min, the recorded current decreased drastically presumably due to fasciculin covalent binding to the serine hydroxyl groups of AChE that could have potentially induce reduced enzymatic activity at the electrode's interface [30]. Fig. 3 (a) shows the DPV graphs at the Fasciculin/AChE/RGO-SnO_2/NPGF electrode where the different

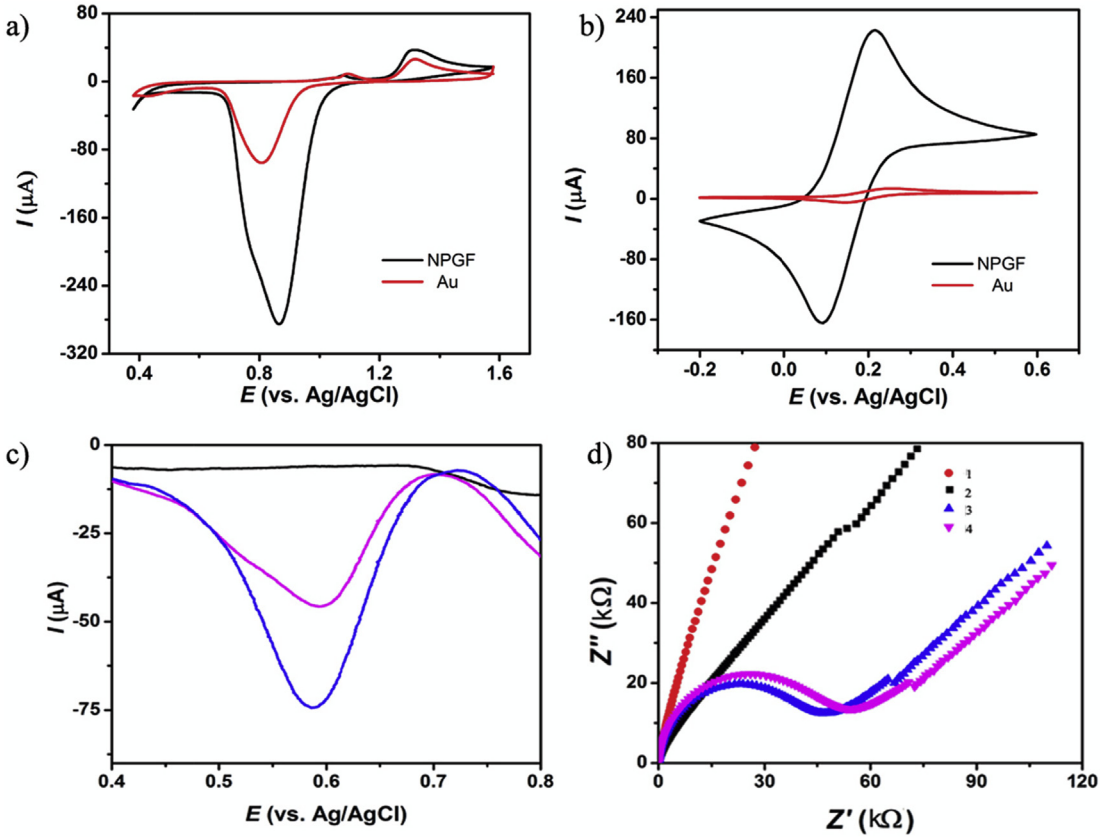

Fig. 2. (a) CV of the Au and NPGF electrodes in 50 mM H_2SO_4. (b) CV for the Au and NPGF electrodes in 50 mM PBS with 50 mM $K_3Fe(CN)_6$ and 10 mM KCl. All electrochemical measurements were performed at a scan rate of 50 mV/s. (c) DPV graph in acetylcholine chloride (AChCl) comtaining solution. (d) EIS graph in $K_3Fe(CN)_6$ containing solution. The color-coding represents NPGF electrode (red), RGO-SnO_2/NPGF electrode (black), AChE/RGO-SnO_2/NPGF electrode (blue) and Fasciculin/AChE/RGO-SnO_2/NPGF electrode (magenta) respectively. (For interpretation of the references to color in this figure legend, the reader is referred to the Web version of this article.)

colors represent different fasciculin concentrations. The oxidation peaks of triocholine appeared on all the modified electrodes, with the decrease in the recorded signal being correlated to the change in fasciculin concentrations. For instance, the peak current at −45.72 μA decreased by 3/5 after the AChE/RGO-SnO_2/NPGF electrode was incubated with 10 nM fasciculin. The peak current at −73.78 μA however stayed almost the same after the AChE/RGO-SnO_2/NPGF electrode was incubated in the control PBS buffer. Fig. 3 (b) inset showed the limit of detection as evaluated using the signal to noise ratios equals to 3, was 8 pM.

In order to evaluate the decrease associated with fasciculin binding, the inhibition rate (I%) was calculated using

$$I\% = \frac{I_{AChE} - I_{Fusciculin}}{I_{AChE}} \times 100\% \quad (3)$$

where I_{AChE} was the peak current of AChCl onto the AChE/RGO-SnO_2/NPGF electrode and $I_{Fasciculin}$ was the peak current recorded at Fasciculin/AChE/RGO-SnO_2/NPGF electrode respectively. Fig. 3 (b) showed the positive correlations between the concentrations of fasciculin and the inhibition rate. Inhibition rates were proportional to the fasciculin concentration in the concentration range from 50 to 100 pM (Fig. 3 (b) insert), where a value of about 0.15% pM for the AChE biosensor sensitivity was obtained from the slope of the linear fitting. Herein the sensitivity of the biosensor was defined as $S = \Delta I\%/\Delta c$, where $\Delta I\%$ represented the change of the inhibition rate and Δc represented the change in fasciculin concentration respectively.

Our analysis also showed that such formed biosensor was selective to the detection of fasiculin. Specifically, control experiments performed with common interfering substances (i.e., biotin and streptavidin [31]; Supporting Information Fig. S2) showed that the biosensor responded by a minimal shift only when fasiculin was contaminated with streptavidin. However, when the interfering substances were placed by themselves on the user-created biosensor [32–34] no changes were noted. The minimal shift was presumably a result of the non-specific binding of streptavidin to fasciculin due to proximal electrostatic interactions [35]. Such contaminant binding was however previously shown to be reduced by increasing ionic strength or decreasing the pH for instance.

Fig. 4 (a) shows the electrode responses before (red) and after (blue) incubation with fasciculin, at different AChCl concentrations. At higher AChCl concentrations the response followed a Michealis–Menten kinetics, with the apparent Michaelis-Menten constant ($K_{M,app}$, which relates to the enzymatic affinity and the ratio of microscopic kinetic constants) being calculated according to the Lineweaver-Burk equation [36] as

$$\frac{1}{I} = \frac{K_{M,app}}{I_{max}} \times \frac{1}{c} + \frac{1}{I_{max}} \quad (4)$$

where c is the concentration of the AChE and I_{max} is the maximum current measured under saturated concentration (Fig. 4 (b)). The saturated concentration was considered the concentration above which all of the binding sites for AChE at the electrode interface are occupied. The saturated current was 26.1 and 20.8 μA, while the

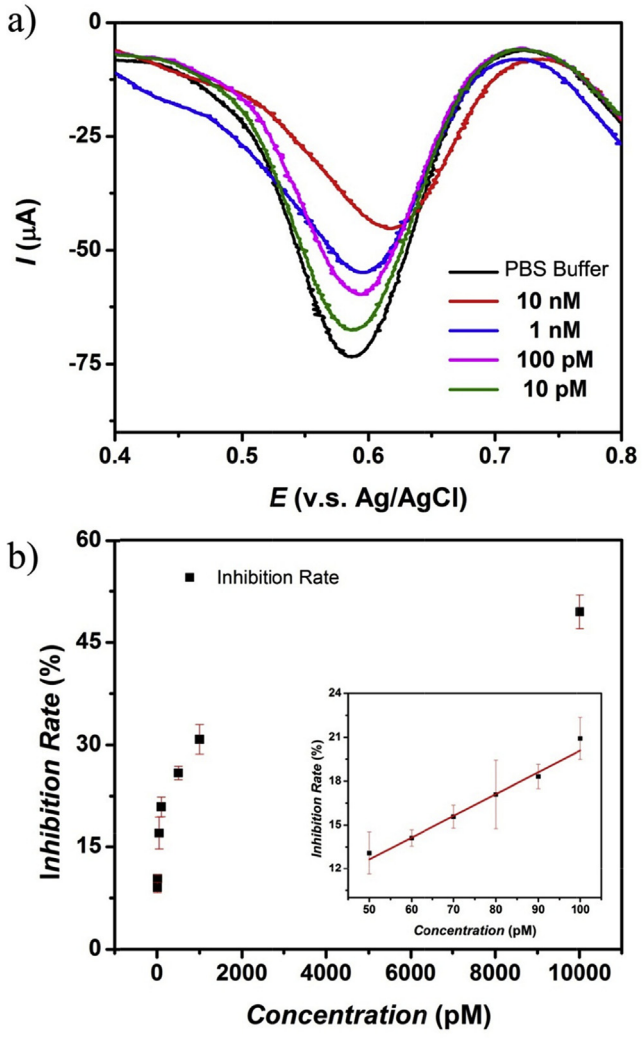

Fig. 3. (a) DPV of Fasciculin/AChE/RGO-SnO_2/NPGF electrode incubated with different concentrations of fasciculin, i.e., 0 M (control PBS, black), 10 nM (red), 1 nM (blue), 100 pM (magenta) and 10 pM (olive green) fasciculin respectively. (b) Relationships between the inhibition rate and fasciculin concentration. Insert: Linear relationship between the inhibition rate and fasciculin concentration in the chosen range of concentrations. (For interpretation of the references to color in this figure legend, the reader is referred to the Web version of this article.)

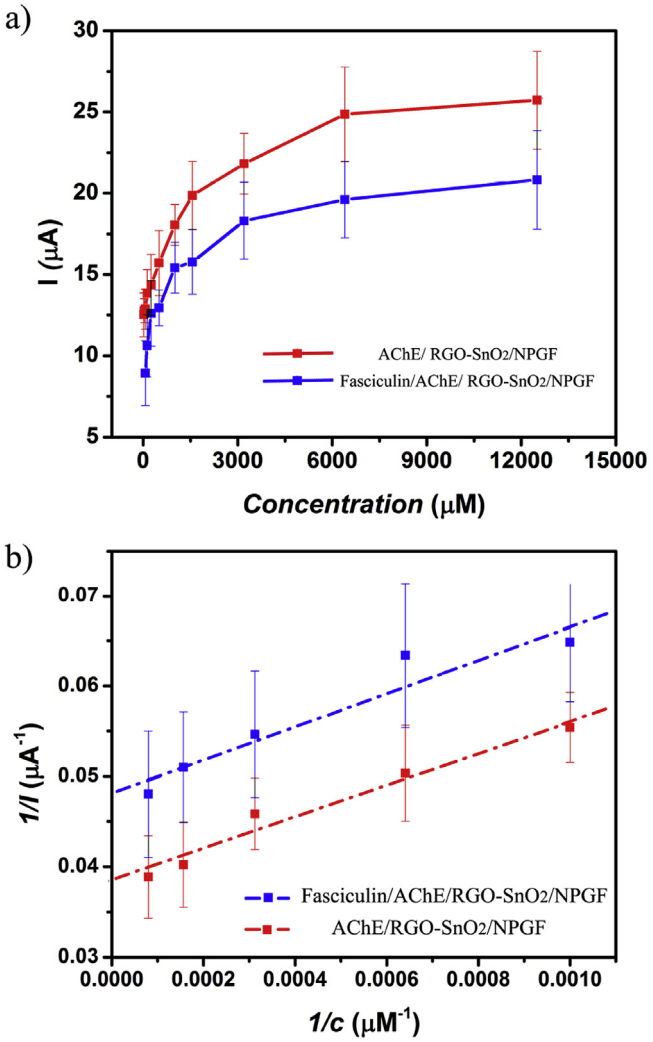

Fig. 4. (a) Current intensity response of the AChE biosensor as a function of AChCl before (red) and after (blue) incubating with fasciculin respectively. (b) The linear part of the curve (a), which was reported as the calibration curve. (For interpretation of the references to color in this figure legend, the reader is referred to the Web version of this article.)

$K_{M,app}$ was about 466.2 μM before AChE inhibition and 390.2 μM after.

The saturated current decreased after fasciculin binding presumably due to the molecule occupying the bioactive sites of the AChCl. A decrease in the $K_{M,app}$ also suggested that the fasciculin was a mixed inhibitor for AChCl [37]. As the non-competitive inhibitor, fasciculin was expected to bind to the AChE and cause changes in the overall 3-dimensional shape of the molecule to lead in a decrease in its activity [38]. Our results are comparable with previous analysis that showed that the $K_{M,app}$ of AChE was about 0.2–1.5 mM after the AChE was inhibited by polyamidoamine dendrimers [39] or 0.369 mM before inhibition by w. somnifera root [40], with the authors of the last study also showing the that $K_{M,app}$ changed with the concentration of the inhibitor (i.e., from 0.425 mM at 0.25 mg/mL to 0.349 mM at 1 mg/mL; Supporting Information Table S1). Moreover, the accuracy of the biosensor calculated as the percentage of biosensor recovery after a known added amount of analyte (i.e, biotin) showed that the recovery of the tested samples was between 105% and 113% (Supporting Information Table S2), which is deemed to be an acceptable degree of accuracy [41,42].

4. Conclusions

We designed and fabricated a highly efficient NPGF-based electrode to be used for detection and inhibition of enzymatic reactions of AChE. The high detection capability (8 pM) in only 30 min incubation time make this electrode not only a viable options for evaluating minimum sample concentrations but further, it eliminates the tedious and laborious labeling processes normally associated with fluorescent techniques for fasiculin inhibition detection. We foresee that the sensitivity limitations inherent to biosensors could be overcome when “array packed integration” of multiple biosensors is to be considered to thus extend the potential of such platforms for other drug-substrates interactions testing.

Acknowledgments

This work was supported by National Science Foundation (NSF) grant 1454230.

Appendix A. Supplementary data

Supplementary data to this article can be found online at https://doi.org/10.1016/j.aca.2019.07.067.

Conflict of interest statement

We declare that we have no financial and personal relationships with other people or organizations that can inappropriately influence our work, there is no professional or other personal interest of any nature or kind in any product, service and/or company that could be construed as influencing the position presented in, or the review of, the manuscript entitled “Nanoporous gold electrode for ultrasensitive detection of neurotoxin fasciculin”.

References

[1] A.s. Association, Alzheimer's disease facts and figures, Alzheimer's Dementia 5 (2009) 234–270 (2009).
[2] M.B. Colovic, D.Z. Krstic, T.D. Lazarevic-Pasti, A.M. Bondzic, V.M. Vasic, Acetylcholinesterase inhibitors: pharmacology and toxicology, Curr. Neuropharmacol. 11 (2013) 315–335.
[3] H. Kaduszkiewicz, T. Zimmermann, H.-P. Beck-Bornholdt, H. van den Bussche, Cholinesterase inhibitors for patients with Alzheimer's disease: systematic review of randomised clinical trials, BMJ 331 (2005) 321–327.
[4] J.S. Birks, L.Y. Chong, J. Grimley Evans, Rivastigmine for Alzheimer's Disease, The Cochrane Library, 2015.
[5] Z. Radić, R. Duran, D.C. Vellom, Y. Li, C. Cervenansky, P. Taylor, Site of fasciculin interaction with acetylcholinesterase, J. Biol. Chem. 269 (1994) 11233–11239.
[6] E. Karlsson, P. Mbugua, D. Rodriguez-Ithurralde, Fasciculins, anticholinesterase toxins from the venom of the green mamba Dendroaspis angusticeps, J. Physiol. (Paris) 79 (1984) 232–240.
[7] K.A. Modesto, C.B. Martinez, Roundup® causes oxidative stress in liver and inhibits acetylcholinesterase in muscle and brain of the fish Prochilodus lineatus, Chemosphere 78 (2010) 294–299.
[8] A. Harvey, A. Anderson, P. Mbugua, E. Karlsson, Toxins from mamba venoms that facilitate neuroiluscular transmission, J. Toxicol. Toxin Rev. 3 (1984) 91–137.
[9] M.-S. García-Ayllón, I. Riba-Llena, C. Serra-Basante, J. Alom, R. Boopathy, J. Sáez-Valero, Altered levels of acetylcholinesterase in alzheimer plasma, PLoS One 5 (2010), e8701.
[10] G.W. Ware, L.A. Albert, D. Crosby, P. Voogt, O. Hutzinger, J.B. Knaak, F.L. Mayer, D. Morgan, D.L. Park, R.S. Tjeerdema, Reviews of Environmental Contamination and Toxicology, Springer, 2006.
[11] Z. Dai, X. Hu, H. Wu, X. Zou, A label-free electrochemical assay for quantification of gene-specific methylation in a nucleic acid sequence, Chem. Commun. 48 (2012) 1769–1771.
[12] Z. Kang, X. Yan, Y. Wang, Y. Zhao, Z. Bai, Y. Liu, K. Zhao, S. Cao, Y. Zhang, Self-powered photoelectrochemical biosensing platform based on Au NPs@ ZnO nanorods array, Nano Res. 9 (2016) 344–352.
[13] Z. Kang, Y. Gu, X. Yan, Z. Bai, Y. Liu, S. Liu, X. Zhang, Z. Zhang, X. Zhang, Y. Zhang, Enhanced photoelectrochemical property of ZnO nanorods array synthesized on reduced graphene oxide for self-powered biosensing application, Biosens. Bioelectron. 64 (2015) 499–504.
[14] S. Chao, E. Krejci, V. Bernard, J. Leroy, L. Jean, P.-Y. Renard, A selective and sensitive near-infrared fluorescent probe for acetylcholinesterase imaging, Chem. Commun. 52 (2016) 11599–11602.
[15] S. Park, J. An, I. Jung, R.D. Piner, S.J. An, X. Li, A. Velamakanni, R.S. Ruoff, Colloidal suspensions of highly reduced graphene oxide in a wide variety of organic solvents, Nano Lett. 9 (2009) 1593–1597.
[16] C. Yu, F. Jia, Z. Ai, L. Zhang, Direct oxidation of methanol on self-supported nanoporous gold film electrodes with high catalytic activity and stability, Chem. Mater. 19 (2007) 6065–6067.
[17] D. Cao, L. Wu, G. Wang, Y. Lv, Electrochemical oxidation behavior of Mg–Li–Al–Ce–Zn and Mg–Li–Al–Ce–Zn–Mn in sodium chloride solution, J. Power Sources 183 (2008) 799–804.
[18] J. Jiang, X. Wang, Fabrication of high-surface nanoporous gold microelectrode, Electrochem. Commun. 20 (2012) 157–159.
[19] F. Jia, C. Yu, Z. Ai, L.J.C.o.M. Zhang, Fabrication of Nanoporous Gold Film Electrodes with Ultrahigh Surface Area and Electrochemical Activity, vol. 19, 2007, pp. 3648–3653.
[20] T. Siepenkoetter, U. Salaj-Kosla, X. Xiao, P.Ó. Conghaile, M. Pita, R. Ludwig, E.J.C. Magner, Immobilization of Redox Enzymes on Nanoporous Gold Electrodes: Applications in Biofuel Cells, vol. 82, 2017, pp. 553–560.
[21] S. Trasatti, O. Petrii, Real surface area measurements in electrochemistry, Pure Appl. Chem. 63 (1991) 711–734.
[22] X. Dong, W. Huang, P. Chen, In situ synthesis of reduced graphene oxide and gold nanocomposites for nanoelectronics and biosensing, Nanoscale Res Lett 6 (2011) 60.
[23] H. Wang, Q. Liang, W. Wang, Y. An, J. Li, L. Guo, Preparation of flower-like SnO2 nanostructures and their applications in gas-sensing and lithium storage, Cryst. Growth Des. 11 (2011) 2942–2947.
[24] X.-Y. Lang, H.-Y. Fu, C. Hou, G.-F. Han, P. Yang, Y.-B. Liu, Q. Jiang, Nanoporous gold supported cobalt oxide microelectrodes as high-performance electrochemical biosensors, Nat. Commun. 4 (2013) 2169.
[25] T. Liu, H. Su, X. Qu, P. Ju, L. Cui, S. Ai, Acetylcholinesterase biosensor based on 3-carboxyphenylboronic acid/reduced graphene oxide–gold nanocomposites modified electrode for amperometric detection of organophosphorus and carbamate pesticides, Sens. Actuators B Chem. 160 (2011) 1255–1261.
[26] F. Li, J. Song, F. Li, X. Wang, Q. Zhang, D. Han, A. Ivaska, L. Niu, Direct electrochemistry of glucose oxidase and biosensing for glucose based on carbon nanotubes@SnO2-Au composite, Biosens. Bioelectron. 25 (2009) 883–888.
[27] F. Li, J. Song, H. Yang, S. Gan, Q. Zhang, D. Han, A. Ivaska, L. Niu, One-step synthesis of graphene/SnO2 nanocomposites and its application in electrochemical supercapacitors, Nanotechnology 20 (2009) 455602.
[28] M. Wei, J. Wang, A novel acetylcholinesterase biosensor based on ionic liquids-AuNPs-porous carbon composite matrix for detection of organophosphate pesticides, Sens. Actuators B Chem. 211 (2015) 290–296.
[29] X. Kang, J. Wang, H. Wu, I.A. Aksay, J. Liu, Y. Lin, Glucose oxidase–-graphene–chitosan modified electrode for direct electrochemistry and glucose sensing, Biosens. Bioelectron. 25 (2009) 901–905.
[30] G. Makhaeva, E. Radchenko, I. Baskin, V. Palyulin, R. Richardson, N. Zefirov, Combined QSAR studies of inhibitor properties of O-phosphorylated oximes toward serine esterases involved in neurotoxicity, drug metabolism and Alzheimer's disease, SAR QSAR Environ. Res. 23 (2012) 627–647.
[31] S. Samarasinghe, F. Meah, V. Singh, A. Basit, N. Emanuele, M.A. Emanuele, A. Mazhari, E.W. Holmes, Biotin interference with routine clinical immunoassays: understand the causes and mitigate the risks, Endocr. Pract. 23 (2017) 989–998.
[32] C.-I. Wang, A.P. Periasamy, H.-T. Chang, Photoluminescent C-dots@ RGO probe for sensitive and selective detection of acetylcholine, Anal. Chem. 85 (2013) 3263–3270.
[33] Q. Zhang, Y. Hu, D. Wu, S. Ma, J. Wang, J. Rao, L. Xu, H. Xu, H. Shao, Z. Guo, S. Wang, Protein-mimicking nanowire-inspired electro-catalytic biosensor for probing acetylcholinesterase activity and its inhibitors, Talanta 183 (2018) 258–267.
[34] F. Ricci, A. Amine, G. Palleschi, D. Moscone, Prussian Blue based screen printed biosensors with improved characteristics of long-term lifetime and pH stability, Biosens. Bioelectron. 18 (2003) 165–174.
[35] G. Johnson, S.W. Moore, Human acetylcholinesterase binds to mouse laminin-1 and human collagen IV by an electrostatic mechanism at the peripheral anionic site, Neurosci. Lett. 337 (2003) 37–40.
[36] Y.-X. Si, S.-J. Yin, D. Park, H.Y. Chung, L. Yan, Z.-R. Lü, H.-M. Zhou, J.-M. Yang, G.-Y. Qian, Y.-D. Park, Tyrosinase inhibition by isophthalic acid: kinetics and computational simulation, Int. J. Biol. Macromol. 48 (2011) 700–704.
[37] G.L. Turdean, Design and development of biosensors for the detection of heavy metal toxicity, Int. J. Electrochem. (2011) 2011.
[38] H. Wu, P. Wang, X. Hu, Z. Dai, X. Zou, Site-selective probe for investigating the asynchronous unfolding of domains in bovine serum albumin, Talanta 84 (2011) 881–886.
[39] B. Klajnert, M. Sadowska, M. Bryszewska, The effect of polyamidoamine dendrimers on human erythrocyte membrane acetylcholinesterase activity, Bioelectrochemistry 65 (2004) 23–26.
[40] S. Kumar, C.J. Seal, E.J. Okello, Kinetics of acetylcholinesterase inhibition by an aqueous extract of Withania somnifera roots, Int. J. Pharm. Sci. Res. 2 (2011) 1188.
[41] E. Commission, Guidance Document on Pesticide Residue Analytical Methods, Directorate Central Health and Consumer Protection, 2010.
[42] V.G. Andreou, Y.D. Clonis, A portable fiber-optic pesticide biosensor based on immobilized cholinesterase and sol–gel entrapped bromcresol purple for in-field use, Biosens. Bioelectron. 17 (2002) 61–69.